Defence Technology 22 (2023) 185–196

Contents lists available at ScienceDirect

Defence Technology

journal homepage: www.keaipublishing.com/en/journals/defence-technology

Resilient tightly coupled INS/UWB integration method for indoor UAV navigation under challenging scenarios

Qian Meng [a], Yang Song [b,*], Sheng-ying Li [a], Yuan Zhuang [c]

[a] Key Laboratory of Micro-Inertial Instrument and Advanced Navigation Technology, Southeast University, Nanjing, 210096, China
[b] Department of Mechanical Engineering, Hong Kong Polytechnic University, Hong Kong, China
[c] State Key Laboratory of Information Engineering in Surveying, Mapping and Remote Sensing, Wuhan University, Wuhan, China

ARTICLE INFO

Article history:
Received 7 November 2022
Received in revised form
8 December 2022
Accepted 20 December 2022
Available online 26 December 2022

Keywords:
Unmanned aerial vehicle (UAV)
Resilient navigation
Indoor positioning
Factor graph optimization
Ultra-wide band (UWB)

ABSTRACT

Based on the high positioning accuracy, low cost and low-power consumption, the ultra-wide-band (UWB) is an ideal solution for indoor unmanned aerial vehicle (UAV) localization and navigation. However, the UWB signals are easy to be blocked or reflected by obstacles such as walls and furniture. A resilient tightly-coupled inertial navigation system (INS)/UWB integration is proposed and implemented for indoor UAV navigation in this paper. A factor graph optimization (FGO) method enhanced by resilient stochastic model is established to cope with the indoor challenging scenarios. To deal with the impact of UWB non-line-of-sight (NLOS) signals and noise uncertainty, the conventional neural net-works (CNNs) are introduced into the stochastic modelling to improve the resilience and reliability of the integration. Based on the status that the UWB features are limited, a 'two-phase' CNNs structure was designed and implemented: one for signal classification and the other one for measurement noise prediction. The proposed resilient FGO method is tested on flighting UAV platform under actual indoor challenging scenario. Compared to classical FGO method, the overall positioning errors can be decreased from about 0.60 m to centimeter-level under signal block and reflection scenarios. The superiority of resilient FGO which effectively verified in constrained environment is pretty important for positioning accuracy and integrity for indoor navigation task.

1. Introduction

Resilient positioning, navigation and timing technology (PNT), which focuses on the convergence of PNT applications with emerging technologies to improve the reliability, continuity and safety of mission-critical applications, is the next frontier of advanced navigation and positioning technologies [1]. A resilient navigation system should generate PNT information adaptable to various complex environments by means of resilient adjustment of functional models and stochastic models to keep accuracy and reliability under challenging scenarios [2]. Based on the redundant information and individualized mechanism, multi-sensor information fusion is the mainstream solution for the resilient navigation [3,4]. In most applications, the implementation of information fusion theory depends on the nominal performance of sensors, where the measurement noise is modeled as white Gaussian noise in system equations and algorithm expression. However, in challenging environments, the performance of state-of-art sensors are limited. For example, the global navigation satellite system (GNSS) receiver in indoor or underground scenarios, the light imaging detection and ranging (LiDAR) and camera under raining or slippery area, the positioning errors of inertial navigation system (INS) accumulate exponentially over time without any external correction [5,6]. What's worse, the above ideal models are no longer working in most cases under challenging scenarios [7]. If we still rely on the nominal model, this model mismatch will cause serious incorrect positioning results and output hazardous mislead information. To reduce vulnerability and ensure reliability, it has become a consensus in resilient PNT to utilize sensors of

* Corresponding author.
E-mail address: 20116167r@connect.polyu.hk (Y. Song).
Peer review under responsibility of China Ordnance Society

https://doi.org/10.1016/j.dt.2022.12.013

opportunity and potential advanced information technologies to meet application-specified navigation requirements in complex and challenging scenarios.

The requirement of unmanned aerial vehicle (UAV) localization and navigation technology in indoor environment has received increasing attentions in recent years as the UAV provides an ideal mobile platform for simultaneous localization and mapping (SLAM), wireless communication and context awareness in closed environment [8,9]. The activities that can benefit from the usage of this technology include defence and rescues, seamless positioning, underground mining, warehouse management, wireless base stations, reconnaissance and surveillance, and so on Refs. [10–13].

The indoor UAV navigation is a classical resilient navigation application as it need to solve the high precision positioning in closed complex buildings [14]. On the one hand the mature navigation systems suitable for open environments such as GNSS/INS integration are not feasible in indoor scenarios due to the lack of availability of GNSS signals. On the other hand, the unknown closed scenarios increase the difficulty of high-precision positioning and leave little room for mistakes. The alternative sensors are required for providing an absolute localization [15]. Based on the high positioning accuracy, low light requirements, low cost and low-power consumption, the ultra-wide band (UWB) technology has got more attentions recently [16,17]. Actually, the positioning principle of UWB is similar to that of GNSS, which uses the line-of-sight (LOS) signals to determine the localization of the receiver. The INS/UWB integration has been widely adopted in indoor pedestrian localization to restrain the INS error divergence based on the centimeter-level measurement precision of UWB [18,19]. Unfortunately, the UWB signal is easy blocked or reflected by objects such as wall and furniture in some unfamiliar or complicated indoor environment [20]. It will result in non-line-of-sight (NLOS) and multipath effect which is shown in Fig. 1. The UWB positioning is susceptible to the above obstructed signals which decreases the performance of INS/UWB integrated system [21]. Due to the three-dimensional flight trajectory and uncertainty of signal reflection, the impact of UWB NLOS and multipath effect on UAV navigation is much worse compared to that of pedestrian localization. To implement high-accuracy and continuous navigation, the system should distinguish the LOS/NLOS signals and adjust the stochastic models to realize optimal signal processing.

Conventionally, the most common information fusion model for INS/UWB integration is extended Kalman filter (EKF), which can deal with the nonlinear models for both UWB positioning and INS [22]. However, for indoor high precision positioning and navigation under indoor challenging scenarios, the EKF overall estimations are suboptimal to meet the performance requirements due to the linearized approximation and the high variance in state estimations and process modelling [23]. Different from the model linear approximation solution of EKF, both the unscented Kalman filter (UKF) and particle filter (PF) are trying to find more accurate estimations through the generation and calculation of a large number of sigma points. The former chooses samples to capture the posterior mean and covariance accurately through the Gaussian random variable, which results in higher order for the nonlinearity [24]. Whereas the latter uses samples to estimate the posterior probability distribution of the state, which gets rid of the limitation of Gaussian distribution [25]. However, for the above methods, the measurements are still limited to the current epoch.

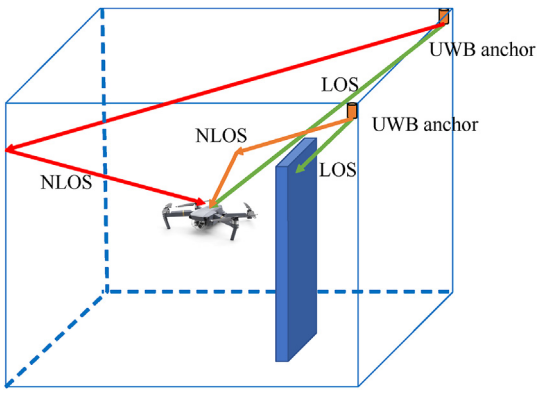

Fig. 1. LOS, NLOS and multipath effect for Indoor UWB positioning.

To overcome the challenge of complex indoor environment to high precision positioning and realize the resilient indoor UAV navigation, a tightly coupled INS/UWB integrated system based on resilient factor graph optimization (FGO) structure is proposed in this paper. Firstly, the information fusion is implemented via factor graph structure to maximize the utilization of historical information and available sensors. Furthermore, to maintain the performance resilience to UWB signal uncertainty, the deep learning method is introduced to the UWB measurements quality control. Particularly, the challenging scenario in this research includes two aspects. Besides the positioning accuracy challenge due to the signal block and reflection, the second one, also the deeper one is the challenge of UWB signal classification and measurements modelling due to the limited UWB features. Based on limited features, two-phase conventional neural networks (CNNs) are designed and implemented in this research. The functional aims of two CNNs are to classify the UWB signal and predict the measurement noise, respectively. The proposed resilient FGO method is tested and effectively verified under actual indoor challenging scenario. The experiment results of tightly coupled INS/UWB integration show that the 'two-phase' CNNs can classify the signals and predict the measurement noise well, the proposed resilient FGO method enhanced by deep learning method can reduce the positioning errors evidently compared to classic EKF and noise-fixed FGO methods. It makes it possible to realize resilient and high-precision UAV navigation in constrained environment. The contributions of this paper can be concluded as follows:

1) Navigation method. For UAV indoor navigation under challenging scenario, a resilient factor graph optimization method for tightly INS/UWB integration is proposed;
2) Resilient solution. Under features-limited scenes, a 'two-phase' conventional neural network (CNNs) solution was designed and implemented for resilient stochastic modelling: one for signal classification and the other one for noise prediction.
3) Constrained environment applicability. The proposed resilient FGO method is tested on flighting UAV platform and effectively verified under actual indoor challenging scenario.

The rest of the paper is organized as follows: Section 2 gave a detailed description of the tightly coupled INS/UWB integration model based on classic factor graph optimization algorithm. Section 3 proposed the resilient factor graph structure enhanced by CNNs structure, including UWB signals classification and measurement noise prediction. Flighting experiment test and performance analysis are given and discussed in Section 4. Finally, Section 5 concluded the research work and contributions.

2. Tightly coupled INS/UWB integration model based on factor graph optimization

The recently resurgence of FGO formulation has started a new revolution for multi-sensor information fusion [26,27]. Compared

to the conventional EKF method, the FGO considers both historical measurements and system updates to optimize the complete state set, which shows better performance in accuracy and robustness. The classical factor graph optimization is described in this section firstly. The tightly coupled INS/UWB integration based on factor graph structure is chosen as the core navigation system for indoor UAV localization in this paper and the navigation system is given in detail latter.

2.1. Factor graph optimization for information fusion

The multi-sensor fusion problem can be modeled as a typical maximum a posteriori (MAP) problem to find the optimal posterior state. Then the probability and corresponding probabilistic relationship can be modeled as 'a factor graph', which is also the origin of its name. It includes two kinds of nodes: factor node and state variables node, respectively. With the above definitions, the factorization of function can be defined as follows:

$$f(\boldsymbol{X}) = \prod_i f_i(\boldsymbol{x}_i) \tag{1}$$

where $\boldsymbol{x}_i$ denotes the set of all state variables nodes involved in factor nodes.

It can be assumed that the variables nodes in the above graph are independent of each other. The measurements and process noise are both modeled as zero-mean Gaussian distribution with the covariance matrices $\boldsymbol{\Sigma}_k$ and $\boldsymbol{\Lambda}_k$, respectively. Based on the Bayes rules and Gaussian model, the formulation can be expressed as follows:

$$\begin{aligned} f(\boldsymbol{x}_k|\boldsymbol{x}_{k-1},\boldsymbol{u}_{k-1}) &\propto p(\boldsymbol{x}_k|\boldsymbol{x}_{k-1},\boldsymbol{u}_{k-1}) \\ &\propto \exp\left(-\frac{1}{2}\|f_k(\boldsymbol{x}_{k-1},\boldsymbol{u}_{\mathrm{k}}) - \boldsymbol{x}_k\|^2_{\boldsymbol{\Lambda}_k}\right) \end{aligned} \tag{2}$$

$$f(\boldsymbol{\gamma}_k|\boldsymbol{x}_k,\boldsymbol{z}_k) \propto p(\boldsymbol{\gamma}_{ik}|\boldsymbol{x}_k,\boldsymbol{z}_{k,i}) \propto \exp\left(-\frac{1}{2}\|h_k(\boldsymbol{x}_k,\boldsymbol{\gamma}_{ik}) - \boldsymbol{z}_{k,i}\|^2_{\boldsymbol{\Sigma}_k}\right) \tag{3}$$

where $\boldsymbol{X} = \{\boldsymbol{x}_k\}$ is estimated state, $\boldsymbol{U} = \{\boldsymbol{u}_k\}$ is control input. $\boldsymbol{Z} = \{\boldsymbol{z}_k\}$ represent the measurements between each landmark $\boldsymbol{\Gamma} = \{\gamma_i\}$ and estimated state.

Substitute Eq. (1) to Eqs. (2) and (3), the factor graph can be further express as a MAP optimization problem.

$$\widehat{\boldsymbol{X}} = \mathrm{argmax}\prod_k p(\boldsymbol{x}_k|\boldsymbol{x}_{k-1},\boldsymbol{u}_{k-1})\prod_k p(\boldsymbol{\gamma}_{ik}|\boldsymbol{x}_k,\boldsymbol{z}_{k,i}) \tag{4}$$

Transforming the above maximization problem into a minimization problem, it can be shown as a nonlinear least square criterion.

$$\widehat{\boldsymbol{X}} = \mathrm{argmin}\left(\sum_{k=1}^{K}\|h_k(\boldsymbol{x}_k,\boldsymbol{\gamma}_{ik}) - \boldsymbol{z}_{k,i}\|^2_{\boldsymbol{\Sigma}_k} + \sum_{i=1}^{L}\|f_k(\boldsymbol{x}_{k-1},\boldsymbol{u}_k) - \boldsymbol{x}_k\|^2_{\boldsymbol{\Lambda}_k}\right) \tag{5}$$

Considering the above nonlinear least square equation, the measurement can be linearized by the Taylor expansion.

$$h_k(\boldsymbol{x}_k,\boldsymbol{\gamma}_{ik}) \approx h_k(\widehat{\boldsymbol{x}}_k,\widehat{\boldsymbol{\gamma}}_{ik}) + \boldsymbol{H}_k(\boldsymbol{x}_k - \widehat{\boldsymbol{x}}_k) + \boldsymbol{J}_k(\boldsymbol{\gamma}_{ik} - \widehat{\boldsymbol{\gamma}}_{ik}) \tag{6}$$

With two Jacobians:

$$\boldsymbol{H}_k = \frac{\partial h(\boldsymbol{x}_k,\boldsymbol{\gamma}_{ik})}{\partial \boldsymbol{x}_k} \tag{7}$$

$$\boldsymbol{J}_k = \frac{\partial h(\boldsymbol{x}_k,\boldsymbol{\gamma}_{ik})}{\partial \boldsymbol{\gamma}_{ik}} \tag{8}$$

Similar to the measurement formula, the process model can be linearized in the same way.

$$f_k(\boldsymbol{x}_{k-1},\boldsymbol{u}_k) \approx f_k(\boldsymbol{x}_{k-1},\boldsymbol{u}_k) + \boldsymbol{F}_{k-1}(\boldsymbol{x}_{k-1} - \boldsymbol{x}_{k-1}) + \boldsymbol{G}_{k-1}\boldsymbol{W}_k \tag{9}$$

With two Jacobians

$$\boldsymbol{F}_{k-1} = \frac{\partial h(\boldsymbol{x}_{k-1},\boldsymbol{u}_k)}{\partial \boldsymbol{x}_{k-1}} \tag{10}$$

$$\boldsymbol{G}_{k-1} = \frac{\partial h(\boldsymbol{x}_{k-1},\boldsymbol{u}_k)}{\partial \boldsymbol{u}_k} \tag{11}$$

Solve the $\widehat{\boldsymbol{X}}$ using Levenberg-Marquardt algorithm (LM) to iteratively obtain the optimal solution.

2.2. INS/UWB integration based on FGO structure

The tightly coupled INS/UWB integration based on FGO structure is described in this subsection. The graph solution of the navigation is shown in Fig. 2. As shown in the figure, the green blocks and orange blocks denote the IMU pre-integration factor and IMU bias factor, respectively. The UWB raw measurements are presented in dark blue circular points. Finally, the purple circular points represent the IMU bias prior factor and initial state prior factor, respectively.

Firstly, for the state space of the system, the state vector is indicated as

$$\boldsymbol{x}_k = \left(\boldsymbol{X}_k^{\mathrm{local}}, \boldsymbol{V}_k^{\mathrm{local}}, \boldsymbol{\Psi}_k^{\mathrm{local}}, \boldsymbol{B}_k^{\mathrm{body}}\right)^{\mathrm{T}} \tag{12}$$

where the right superscript and right subscript represent the reference coordinate system and positioning epochs. $\boldsymbol{X}_k^{\mathrm{local}}$, $\boldsymbol{V}_k^{\mathrm{local}}$ and $\boldsymbol{\Psi}_k^{\mathrm{local}}$ represent the measurements of the UWB receiver, the velocities and orientations of UAV in local frame at epoch k, respectively. $\boldsymbol{B}_k^{\mathrm{body}}$ represents the bias of accelerometer and gyroscope of IMU in the body frame at epoch k.

The raw UWB measurements are utilized as UWB range factor in this FGO structure. The predicted measurement $\boldsymbol{z}_{k,i}^{\mathrm{UWB,Range}}$ from the ith anchor and the corresponding the UWB range factor $f_{\mathrm{UWB}}^{\mathrm{Range}}(\boldsymbol{x}_k)$ can be calculated as follows:

$$\boldsymbol{z}_{k,i}^{\mathrm{UWB,Range}} = h^{\mathrm{Range}}(\boldsymbol{x}_k,\boldsymbol{\gamma}_{ik}) = \|\boldsymbol{\gamma}_{ik} - \boldsymbol{x}_k\|_2 + \boldsymbol{n}_{\mathrm{range}}^{\mathrm{UWB}} \tag{13}$$

$$f_{\mathrm{UWB}}^{\mathrm{Range}}(\boldsymbol{x}_k) = \left\|\boldsymbol{z}_{k,i}^{\mathrm{UWB,Range}} - h^{\mathrm{Range}}(\boldsymbol{x}_k,\boldsymbol{\gamma}_{ik})\right\|^2_{\boldsymbol{\Sigma}_k^{\mathrm{Range}}} \tag{14}$$

where $\boldsymbol{\gamma}_{ik}$ represents the position of the ith anchor at time k. $\boldsymbol{\Sigma}_k^{\mathrm{Range}}$ denotes the covariance matrix corresponding to the UWB range measurement model.

The INS function, usually working as inertial measurement unit

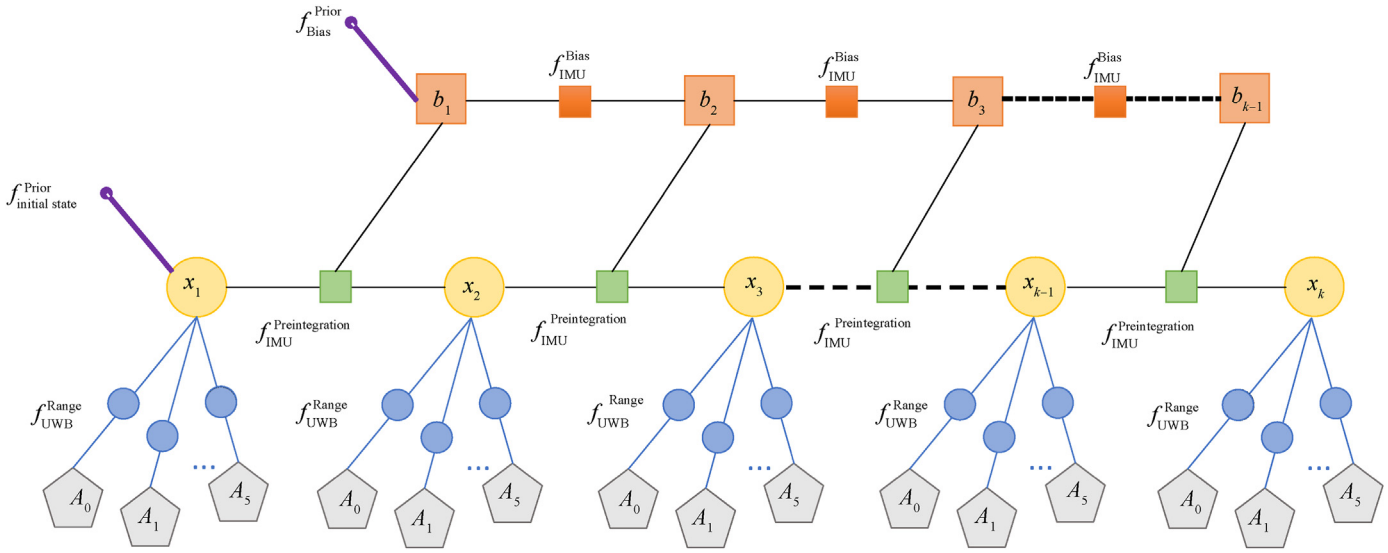

Fig. 2. Tightly coupling UWB/INS integration based on FGO.

(IMU) in the hardware platforms, contains a three-dimensional accelerometer and three-dimensional gyroscope that can measure the rotation and acceleration of the body. For the IMU measurement factor, the output frequency of IMU is much greater than that of UWB. It will result in a large number of IMU factor nodes between two UWB factor nodes if the state $\boldsymbol{x}_k$ is predicted directly with the IMU raw measurements and the state estimation of $\boldsymbol{x}_{k-1}$. To avoid the difficulties of the implementation of massive factor nodes and the corresponding undesirable computational burden. The pre-integration technology is accepted in our tightly coupled INS/UWB integration method to improve the factor graph optimization [28,29]. Thus, the IMU pre-integration factor and the time relationship with UWB factor can be shown in the following figure (see Fig. 3).

As shown in the figure, the basic principle of pre-integration is not difficult to understand. Successive IMU measurements are integrated between two epochs and result in a new IMU pre-integration factor for FGO. The time synchronization problem with UWB measurements can also be solved in this processing. The IMU integration can be iterated along all the time duration Δt as follows:

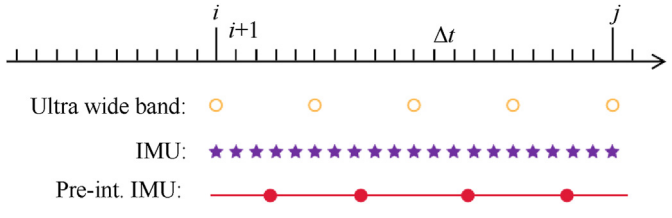

Fig. 3. Schematic diagram of IMU pre-integration factor.

$$\begin{aligned}
\boldsymbol{R}_j &= \boldsymbol{R}_i \prod_{k=i}^{j-1} \mathrm{Exp}\left[\left(\tilde{\omega}_k - \boldsymbol{b}_g^k - \boldsymbol{\eta}_{gd}^k\right)\Delta t\right] \\
\boldsymbol{v}_j &= \boldsymbol{v}_i + \boldsymbol{g}\Delta t_{ij} + \sum_{k=i}^{j-1} \boldsymbol{R}_k\left(\tilde{\boldsymbol{a}}_k - \boldsymbol{b}_a^k - \boldsymbol{\eta}_{ad}^k\right)\Delta t \\
\boldsymbol{P}_j &= \boldsymbol{P}_i + \sum_{k=i}^{j-1}\left[\boldsymbol{V}_k\Delta t + \frac{1}{2}\boldsymbol{g}\Delta t^2 + \frac{1}{2}\boldsymbol{R}_k\left(\tilde{\boldsymbol{a}}_k - \boldsymbol{b}_a^k - \boldsymbol{\eta}_{ad}^k\right)\Delta t^2\right]
\end{aligned} \tag{15}$$

where the $\boldsymbol{R}_i, \boldsymbol{v}_i$, and $\boldsymbol{P}_i$ denote the rotation, velocity and position parameters of IMU in frame$i$, respectively. $\boldsymbol{b}_g^k$ and $\boldsymbol{b}_a^k$ represent the biases of angular velocity and acceleration, respectively. $\boldsymbol{\eta}_{gd}^k$ and $\boldsymbol{\eta}_{ad}^k$ denote the random noise of IMU measurement. Then, to further avoid recomputing the above integration due to the UWB update, the following relative motion increments are introduced into the detailed processing to complete the update of IMU measurement between the two UWB epochs:

$$\begin{aligned}
\Delta\boldsymbol{R}_{ij} &= \prod_{k=i}^{j-1} \mathrm{Exp}\left(\left(\tilde{\omega}_k - \boldsymbol{b}_g^k - \boldsymbol{\eta}_{gd}^k\right)\Delta t\right) \\
\Delta\boldsymbol{v}_{ij} &= \sum_{k=i}^{j-1} \Delta\boldsymbol{R}_{ik}\left(\tilde{\boldsymbol{a}}_k - \boldsymbol{b}_a^k - \boldsymbol{\eta}_{gd}^k\right)\Delta t \\
\Delta\boldsymbol{P}_{ij} &= \sum_{k=i}^{j-1}\left[\Delta\boldsymbol{V}_{ik}\Delta t + \frac{1}{2}\Delta\boldsymbol{R}_{ik}\left(\tilde{\boldsymbol{a}}_k - \boldsymbol{b}_a^k - \boldsymbol{\eta}_{ad}^k\right)\Delta t^2\right]
\end{aligned} \tag{16}$$

where $\Delta\boldsymbol{R}_{ik} \doteq \boldsymbol{R}_i^{\mathrm{T}}\boldsymbol{R}_k$ and $\Delta\boldsymbol{v}_{ik} \doteq \boldsymbol{R}_i^{\mathrm{T}}(\boldsymbol{v}_k - \boldsymbol{v}_i - \boldsymbol{g}\Delta t_{ik})$.

About the measurement noise after IMU pre-integration, the first-order approximation is introduced to calculate the noise

propagation and biases changes $b \leftarrow \bar{\boldsymbol{b}} + \delta \boldsymbol{b}$. The cost function in factor graph optimization of IMU pre-integration model and observed values are accepted to calculate the residual of IMU pre-integration factor, which are defined as

$$
\begin{aligned}
\boldsymbol{r}_{\Delta \mathbf{R}_{ij}} &\doteq \lg\left(\left(\Delta\widetilde{\boldsymbol{R}}_{ij}\left(\bar{\boldsymbol{b}}_g^i\right)\operatorname{Exp}\left(\frac{\partial\left(\Delta\widetilde{\boldsymbol{R}}_{ij}\left(\bar{\boldsymbol{b}}_g^i\right)\right)}{\partial \boldsymbol{b}_g}\delta\boldsymbol{b}_g^i\right)\right)^{\mathrm{T}}\boldsymbol{R}_i^{\mathrm{T}}\boldsymbol{R}_j\right) \\
\boldsymbol{r}_{\Delta \mathbf{v}_{ij}} &\doteq \boldsymbol{R}_i^{\mathrm{T}}\left(\boldsymbol{v}_j - \boldsymbol{v}_i - \boldsymbol{g}\Delta t_{ij}\right) - \left[\Delta\widetilde{\boldsymbol{v}}_{ij}\left(\bar{\boldsymbol{b}}_g^i, \bar{\boldsymbol{b}}_a^i\right) + \frac{\partial\left(\Delta\widetilde{\boldsymbol{v}}_{ij}\left(\bar{\boldsymbol{b}}_g^i, \bar{\boldsymbol{b}}_a^i\right)\right)}{\partial \bar{\boldsymbol{b}}_g}\delta\boldsymbol{b}_g^i + \frac{\partial\left(\Delta\widetilde{\boldsymbol{v}}_{ij}\left(\bar{\boldsymbol{b}}_g^i, \bar{\boldsymbol{b}}_a^i\right)\right)}{\partial \bar{\boldsymbol{b}}_a}\delta\boldsymbol{b}_a^i\right] \qquad \boldsymbol{r}_{ba} = \boldsymbol{b}_j^a - \boldsymbol{b}_i^a \; \boldsymbol{r}_{bg} = \boldsymbol{b}_j^g - \boldsymbol{b}_i^g \\
\boldsymbol{r}_{\Delta \mathbf{P}_{ij}} &\doteq \boldsymbol{R}_i^{\mathrm{T}}\left(\boldsymbol{p}_j - \boldsymbol{p}_i - \boldsymbol{v}_i\Delta t_{ij} - \frac{1}{2}\boldsymbol{g}\Delta t_{ij}^2\right) - \left[\Delta\widetilde{\boldsymbol{P}}_{ij}\left(\bar{\boldsymbol{b}}_g^i, \bar{\boldsymbol{b}}_a^i\right) + \frac{\partial\left(\Delta\widetilde{\boldsymbol{p}}_{ij}\left(\bar{\boldsymbol{b}}_g^i, \bar{\boldsymbol{b}}_a^i\right)\right)}{\partial \bar{\boldsymbol{b}}_g}\delta\boldsymbol{b}_g^i + \frac{\partial\left(\Delta\widetilde{\boldsymbol{p}}_{ij}\left(\bar{\boldsymbol{b}}_g^i, \bar{\boldsymbol{b}}_a^i\right)\right)}{\partial \bar{\boldsymbol{b}}_a}\delta\mathbf{b}_a^i\right]
\end{aligned}
\tag{17}
$$

where the $\Delta\tilde{\boldsymbol{R}}_{ij}\Delta\tilde{\boldsymbol{v}}_{ij}\Delta\tilde{\boldsymbol{P}}_{ij}$ represent the IMU pre-integration rotation, velocity and position measurements between keyframe*i* and*j*, respectively. $\boldsymbol{r}_{\Delta \boldsymbol{R}_{ij}}$, $\boldsymbol{r}_{\Delta \boldsymbol{v}_{ij}}$, $\boldsymbol{r}_{\Delta \boldsymbol{P}_{ij}}$, $\boldsymbol{r}_{ba}$ and $\boldsymbol{r}_{bg}$ respectively represent the corresponding rotation constraint, velocity constraint, position constraint, the accelerometer and gyroscope biases constraints. 'Exp' 'log' are the exponential and logarithm map operators, respectively. The step-by step specification about IMU pre-integration can be referred to our previous paper [30].

3. Resilient stochastic model for factor graph optimization

One of the characteristics of resilient navigation is that it requires the autonomous navigation system to maintain the system integrity and continuity under disturbed conditions by means of redundant information or backup system. To achieve the above goals, the crucial work is to manage the stochastic model of navigation sensors against model misspecification, signal interference and sensor faults [31,32]. For the proposed tightly coupled INS/UWB FGO structure, the classical solution is that the state propagation process noise and measurement covariance matrix corresponding to INS and UWB are fixed values, which allows the FGO to use the measured values to calculate the new state with constant weights. When UAV is operating in an empty and unobstructed indoor environment, the operating state of each sensor is basically stable. It is normal to employ a fixed weight to update the new state of UAV. By artificially calibrating the characteristic of various sensors, the appropriate process noise covariance matrix and measurement noise covariance matrix can be effectively designed, which makes it application in most scenarios.

However, when the UAV is operating in a challenging environment, such as indoor pipeline monitoring and cargo transportation, it will deal with a more complicated indoor scenario. Although the IMU has little dependence on the external environment, the UWB will be highly affected with a poor environment and induce a large error in range measurement. Therefore, in this case, the UAV may perform a wrong action, due to the highly large positioning error.

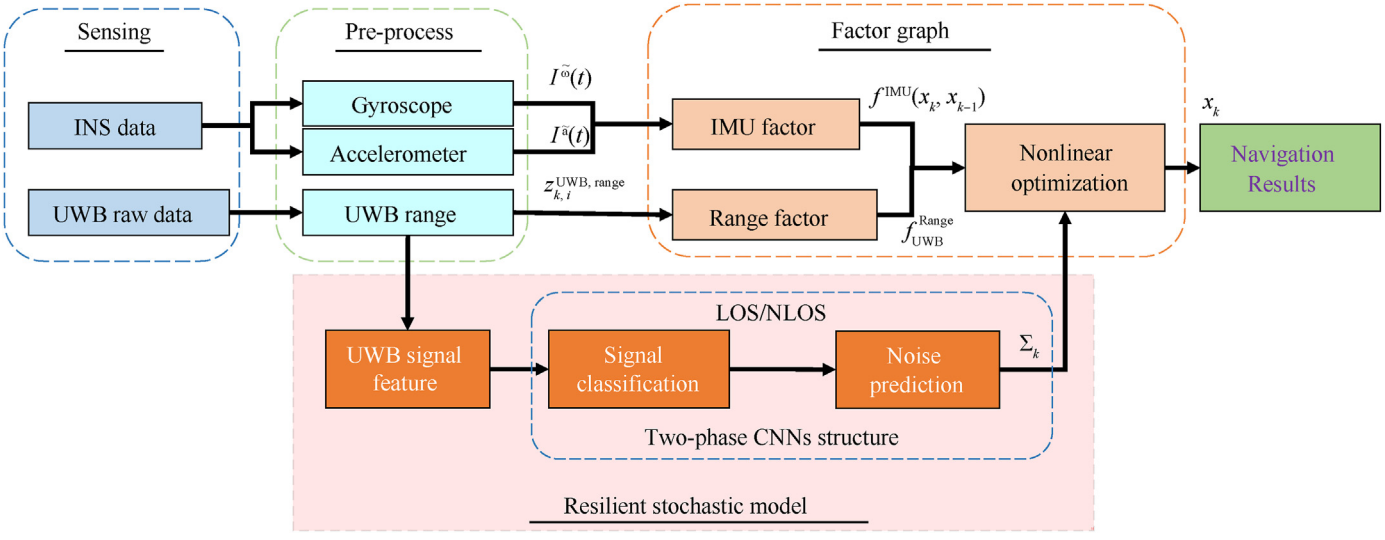

Fig. 4. Tightly coupled INS/UWB integration enhanced by resilient factor graph optimization.

As a result, in order to obtain a better positioning accuracy and maintain the navigation continuity in a challenging indoor scenario, the core solution in this research is to distinguish the quality of UWB signals and predict the value of measurement noise covariance matrix. Thus a tightly coupled INS/UWB integration enhanced by resilient factor graph optimization is proposed and designed in this section. The framework of the proposed method is shown in Fig. 4. It mainly includes three modules: Sensing signal pre-processing; factor graph optimization-based navigation and resilient stochastic model based on two-phase CNNs structure. The INS and UWB signal pre-processing and tightly coupled INS/UWB integration based on FGO have been elaborated in the above sections. The following parts will focus on the implementation of resilient stochastic model and the corresponding UWB signal classification and noise prediction.

3.1. UWB receiver output feature

For UWB measurement system, the UWB receiver is connected to the *Intel* Up Board, and the measurement can be directly saved in the form of date packet by Robot Operating System (ROS) to help user check and operation. Therefore, from the collected data packets, we can view the output measurement types of UWB, and further use these measurements to evaluate the quality of the current environment to achieve signal classification and noise prediction. Unfortunately, different from the GNSS signals outside, the basic UWB system cannot provide some raw but important features such as signal gain, time delay, amplitude and code/carrier phase. The features for classifying and prediction are pretty limited.

Hence, in consideration of the above limitations, the selected UWB signal features are listed in Table 1. The UWB range measurement is the first choice as it directly determines the accuracy of positioning results, The fp_rssi and rx_rssi are the transmitted power and received power, since the power loss of signal will increase when it is blocked or reflected, thus these features may have relationship with the type of signals and measurements noise. Besides that, the anchor base station coordinates are introduced as feature information to improve the difference between the features.

After collecting the useable data, the deep learning method is employed for UWB signal classification and measurement noise prediction in the following subsections. In the deep learning methods, based on the characteristics of weight sharing and local connectivity, the convolutional neural networks (CNNs) have already got rising attentions and successful applications in many fields. The CNNs explore the spatial correlation between selected features. By introducing the operation of convolution kernel, the number of parameters is greatly reduced. Rectified Linear Unit (ReLU) activation layer, batch normalization layer (BN) and residual block have appeared successively and are widely used in target detection and classification. After the convolutional layer is completed, all the extracted features will be arranged in a column vector, and then the classification result is output through the fully connected layer. Compared with traditional neural networks, CNNs can achieve weight sharing, thus it has faster learning efficiency. In our search, the CNNs structure is chosen for UWB measurement classification and noise prediction.

Table 1
Selected features for UWB signals classification and prediction.

No.	Feature	Remarks
1	$z_{k,i}^{\mathrm{UWB,Range}}$	The range measurements between the receiver and ith anchor at time k
2	fp_rssi	First path power level. Unit: dB
3	rx_rssi	Received Power level Unit: dB
4	P_{anch}	UWB Anchor Position (Unit: m) $P_{\mathrm{anch}} = (x_{\mathrm{anch}} \quad y_{\mathrm{anch}} \quad z_{\mathrm{anch}})$

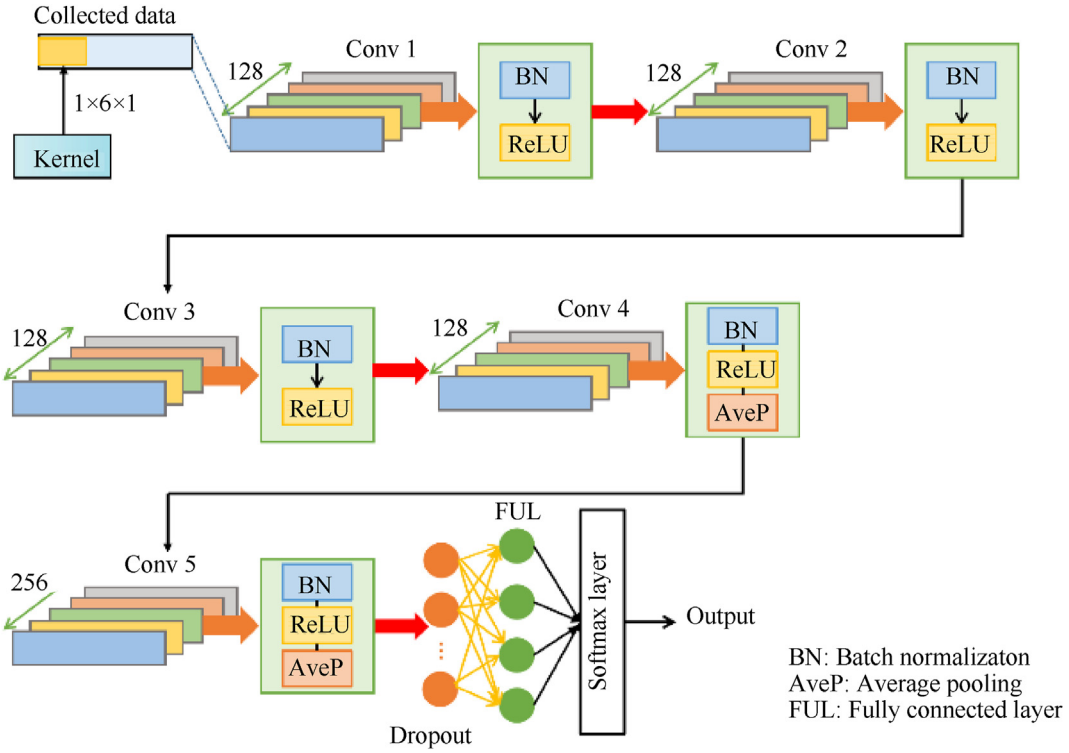

Fig. 5. Signal Classification Network structure. 'Conv' represents the convolution layer, the green numbers denote the numbers of kernel from Conv1 to Conv 5, respectively.

3.2. Phase I: UWB measurement classification

Based on the collected UWB measurement information, a brief assessment of signal quality and operating circumstance can be conducted, such as clear corresponding to open and interference corresponding to dense, and further predicting noise based on classification results. Before correcting different measurement noise covariance matrix to adapt to various environments to achieve adaptive adjustment, the first task is to use the UWB measurements to identify the operating scenes and classify the signal. The proposed signal classification network is shown in Fig. 5. It contains 5 CLs, 1 dropout layer and 1 fully connected layer. As shown in the figure, the first three CLs is built of three functional stages, i.e., convolution, batch normalization and ReLU activation function. However, the pooling operation is not introduced, due to the original data is just a row vector with 6 elements (the anchor position is regarded as three elements in the input vector), even if it is convolved 128 times in one convolutional layer, the extracted feature information is not inefficiency. In order to retain more valid data, thus in the first three CLs, pooling operation cannot be adopted. For the last two CLs, since the number of extracted features is sufficient, in order to improve the learning efficiency, average pooling is employed to down sample. Dropout layer is similar to the pooling operation, which remove half of parameters randomly for increasing the training speed. Finally, a fully connected layer is connected to the softmax neuron to output the classification probability.

After designing the network, the next step is to train and evaluate its performance. The loss function is used in this training processing. For classification problem, the cross-entropy loss is widely used, which can be expressed as follow:

$$L = -\sum_i y_i^{'} \lg (y_i) \tag{18}$$

where $y_i^{'}$ is the ground truth label of the ith training date, and y_i is the prediction results of the training data.

As shown in Fig. 6, after 800 iterations, the classification accuracy of test set is close to 80%. The ground truth acquisition method will be described in the experiment section. Actually it is not an ideal result for signal classification. However considering of the limited features, it is an acceptable number.

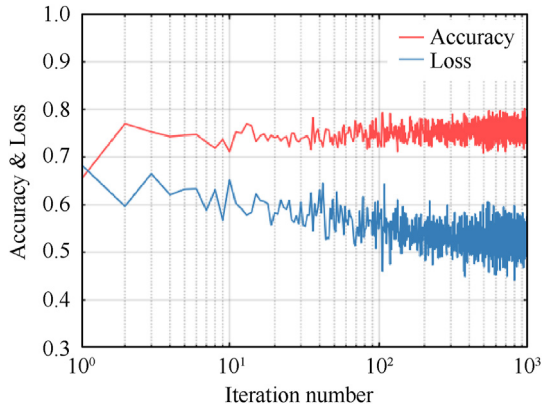

Fig. 6. Training process of classification network.

3.3. Phase II: UWB measurement noise prediction

As analyzed in the above subsection, most NLOS signals have been excluded after signal classification phase, which will improve the position precision apparently. However due to the limited features, some NLOS signals still left in the data. Besides the signal reflection, the measurement noise is another important parameter

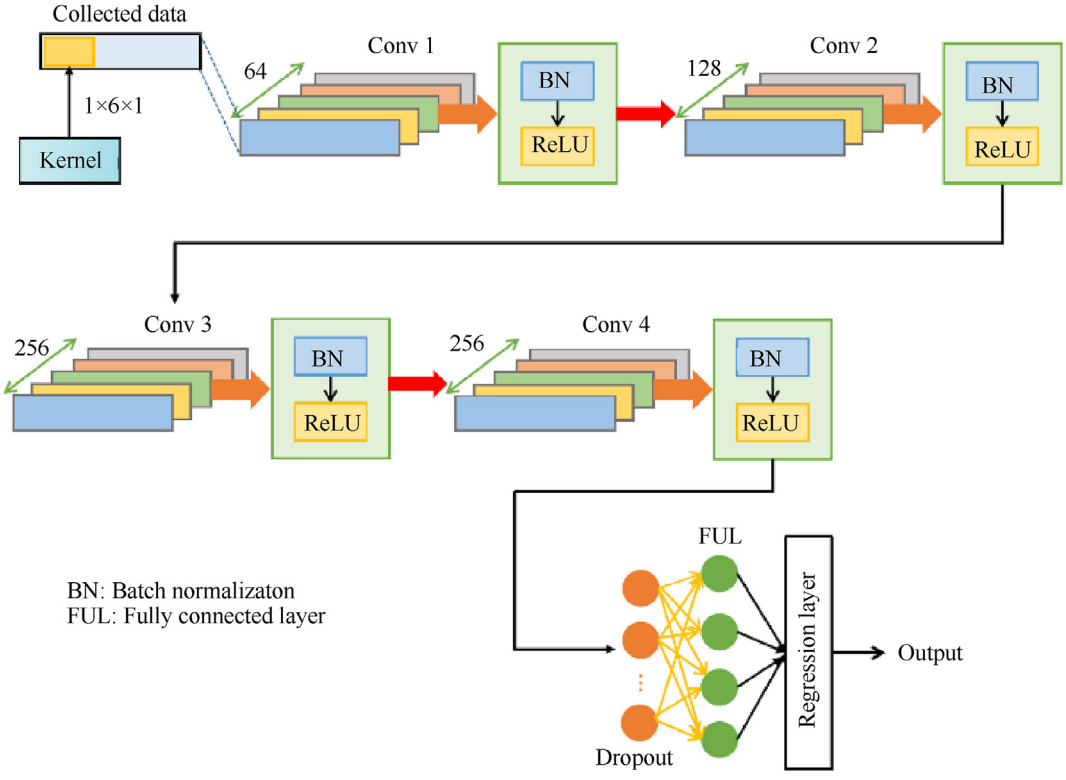

Fig. 7. Noise Prediction Network Structure. 'Conv' represents the convolution layer. The green numbers denote the numbers of kernel from Conv1 to Conv 4, respectively.

that affects the signal quality of UWB measurements. To implement resilient navigation in challenging scenarios, a noise prediction network is built in the second phase. The motivation of the second network includes two aspects: the first one is to obtain the exact value of UWB measurement noise covariance matrix. The second aspect is to regard the residual NLOS signals as noise to reduce its impact on positioning performance.

As shown in Fig. 7, the CNNs in the second phase contains 4 CLs, 1 dropout layer and 1 fully connected layer. Different from the UWB signal classification network, all the CLs are constructed of three functional stages, i.e., convolution, batch normalization and ReLU activation function. For the first CLs, the 64 convolution kernels are used to extract information from the input data to generate a new feature map. Then, through batch normalization, the newly generated feature date becomes Gaussian distribution, which assist the date in the source space and target space to maintain a consistent distribution. Subsequently, a nonlinear transformation is introduced into the model by using the ReLU activation function, which enables our network to fit the nonlinear relationship between the input data and output results.

To select suitable parameters, we take Loss and root mean square error (RMSE) as indicators of concern, conduct several sets of experiments, and select appropriate parameters. After studying different combinations of kernel numbers and trying different combinations of kernel sizes, the case of (64, 128, 128, 256) is selected as the final parameter finally. The training process of noise prediction is shown in Fig. 8. It is encouraging that the noise level predicted in the test set is basically consistent with the ground truth. The RMSE used for describing the prediction error is as follows:

$$\mathrm{RMSE} = \sqrt{\frac{\sum_{k=1}^{n}(\hat{y}_k - y_k)^2}{n}} \tag{19}$$

where $\hat{y}_k$ denotes the prediction value of UWB measurement noise and y_k represents the labeled value of training set.

4. Experimental tests and results analysis

4.1. Experiment setup and data collection

The experimental setting and UAV flighting tests were conducted in the building indoor environment and the corresponding experimental scene and UAV platform are shown in Fig. 9. Particularly, to maintain the system accuracy in vertical direction, the vertical dilution of precision (VDOP) concept of GNSS is introduced into the location of UWB anchors and the optimal VDOP is carefully considered in this research to locate the spatial distribution of anchors [33]. Blackboards and Television are chosen as artificial obstacles to result in the reflections of the UWB signals. The positioning performance of EKF and proposed FGO method will be evaluated under this actual indoor challenging environment.

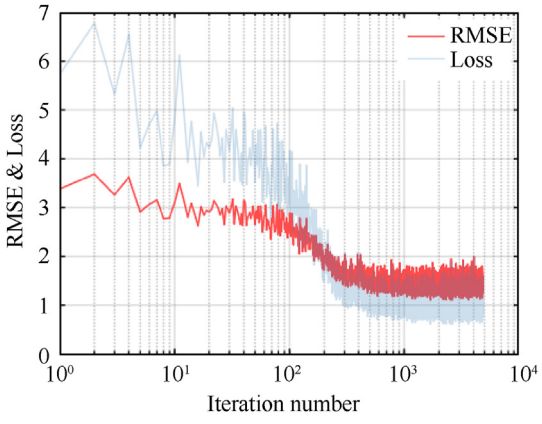

Fig. 8. Training process of noise prediction network.

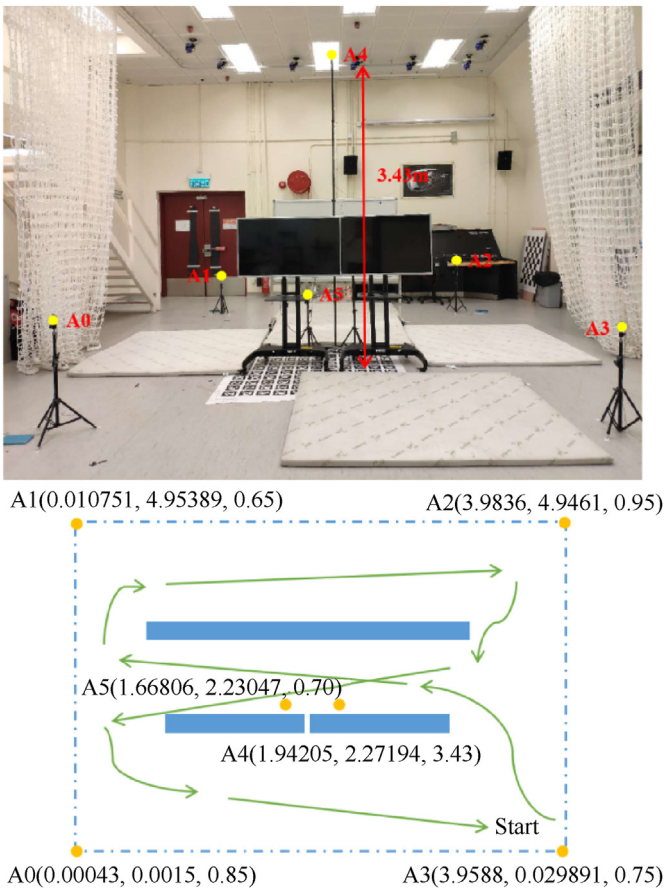

Fig. 9. Experiment setup and flight path.

The specifications of UWB receiver and IMU are shown in Fig. 10, Tables 2 and 3, respectively. In addition, an eight-camera motion capture analysis system (VICON), was introduced into the experiments to provide the ground truth of UAV dynamic position and furthermore the basic criterion for UWB signal classification. Three integration models: EKF, classical FGO and proposed resilient FGO are conducted and compared in indoor challenging environment.

4.2. Experiments under indoor open scenario

The UAV experiments under relative open scenario were tested firstly. The motivations of open scenario test before challenging scenario included two aspects: to verify the applicability of the proposed tightly coupled FGO structure for INS/UWB integration and to tuning the optimal parameter for two methods to show the nominal performance. As shown in Fig. 11, the flight path begins from the bottom right corner in experiment scenario and turns counterclockwise back to the terminal point near the start point. Fig. 12 and Table 4 show the positioning performance and results errors. The statistical data related to positioning performance include error means and standard deviation (STD).

As shown in the figure and table, for the integration based on EKF, the horizontal and vertical errors are 0.066 m and 0.051 m

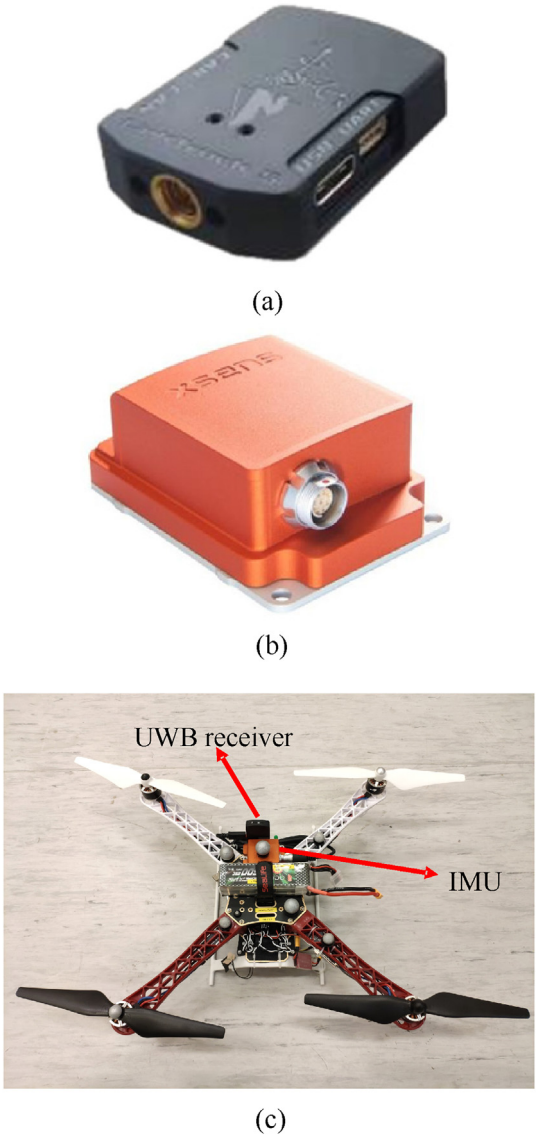

Fig. 10. UAV platform and data collection: (a) LinkTrack S UWB receiver; (b) Xsens Mti-10 IMU; (c) UAV platform.

with a standard deviation of 0.044 m and 0.085 m, respectively. Compared to those of EKF, the FGO method has some improvements in both horizontal and vertical directions. The overall error and standard deviation decrease from 0.092 m to 0.088 m–0.070 m and 0.042 m respectively. Particularly the improvements in

Table 2
Link Track S specifications.

No.	Item	Details
1.	Antenna Types	Built-in onboard antenna
2.	Product size/mm^3	43*31*10
3.	Communication distance/m	80
4.	Supply voltage/V	(3.6, 5.5)
5.	Operating frequency band/GHz	(3744, 4243.2) (4243, 4742.4) (6240, 6739.2)
6.	Communication interface	USB, UART, CAN
7.	One. Two-dimensional positioning accuracy/cm	10
8.	Three-dimensional positioning accuracy/cm	30

Table 3
Xsens Mti-10 specifications.

No.	Item	Details
1.	Input voltage/V	4.5–34 or 3V3
2.	Output frequency/kHz	Up to 2
3.	Latency/ms	<2
4.	Supply voltage/V	(3.6, 5.5)
5.	Standard full range gyro/((°)s^{-1})	450
6.	communication interface	USB、UART、CAN
7.	In-run bias stability gyro/((°)h^{-1})	18
8.	Bandwidth acc	Bandwidth acc
9.	Typical power consumption/mW	400–550
10.	Temperature/°C	−40 to 85
11.	Sampling frequency	10 kHz/channel (60 kS/s)
12.	Clock Drift	10 ppm or external reference
13.	communication interface	RS232/RS485/RS422/UART/USB

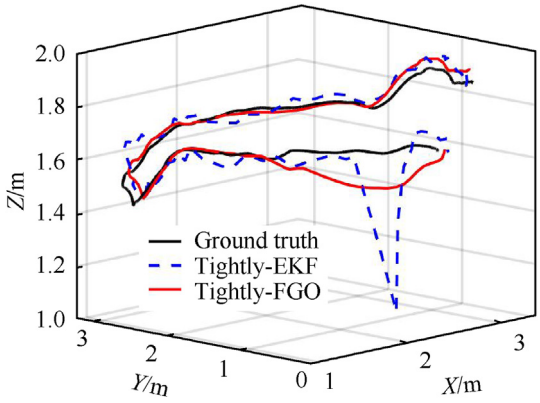

Fig. 11. Fight trajectory and positioning results of two methods under open scenario.

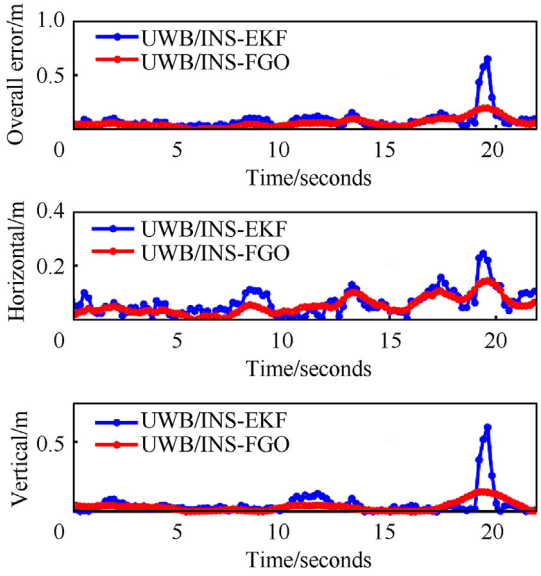

Fig. 12. Positioning results and errors of two methods under open scenario.

standard deviations are pretty obvious compared to those in error means.

It cannot be ignored that there's an obvious peak in the performance of EKF positioning results near the terminal point. It results an outlier in the flighting trajectory due to the UWB signal fault and resulted in a big positioning failure. On the other hand, the FGO method can effectively reduce the impact of this outlier. It

Table 4
Positioning performance of two methods under indoor open scenario.

Position errors/meters		EKF	FGO
Overall error	Mean	0.092	0.070
	Standard deviation	0.088	0.042
Horizontal component	Mean	0.066	0.056
	Standard deviation	0.044	0.031
Vertical component	Mean	0.051	0.036
	Standard deviation	0.085	0.035

shows the superiority of FGO once again that compared to the approximation of Jacobians every epoch in Kalman filter theory, the FGO method aims to re-linearize iteratively to minimize the cost function to search the optimal solution. That is the essential difference between optimization and filtering. Compared to Kalman filter, which uses only last-step states and current measurements to estimate current states, FGO is essentially smoother by using multiple epochs of measurements and states to estimate current states, which is effective in resisting the outlier. The improvements in standard deviations of positioning errors also benefit from this information processing.

4.3. Experiments under indoor challenging scenario

For the indoor challenging scenario, the UAV flighted through the blackboard and Television. The UWB signals were blocked and reflected by the artificial obstacles. Beginning from the lower right corner, the UAV completed the Arabic number eight-shaped path and flighted continuously back to the start point. The trajectory and positioning results under this challenging scenario was shown in Figs. 13 and 14. The detailed positioning errors are shown in Table 5.

The impact of UWB signal block and reflection on positioning accuracy is obvious for both EKF and FGO. The horizontal and vertical errors of EKF are 0.610 m and 0.386 m, respectively. On the other hand, the corresponding values of FGO is 0.519 m and 0.335 m. Compared to EKF, the FGO method shows some resilience to challenging scenarios and the position trajectory is much smoother than that of EKF (the standard deviation is 0.196 m for the former and 0.422 m for the latter). However once the faulty observations exist in almost every epoch, it is difficult to calculate the optimal solution in cost function model involving so many faulty measurements. The above sub-meter level position accuracies are apparently not unacceptable for indoor flight. It is easy to deviate from the target and even collide with the buildings. To maintain the navigation accuracy of open environment in such complex indoor scenarios, it is necessary to distinguish the quality of limited UWB signal.

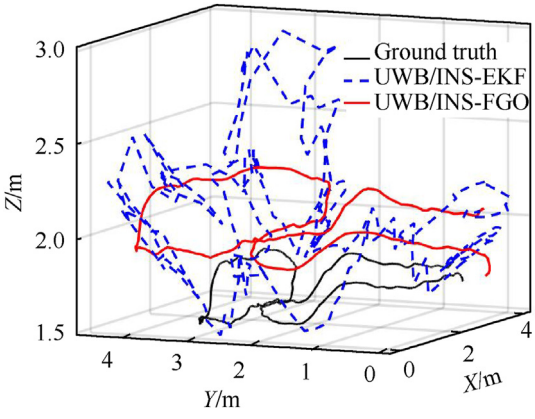

Fig. 13. Fight trajectory and positioning results under challenging scenario.

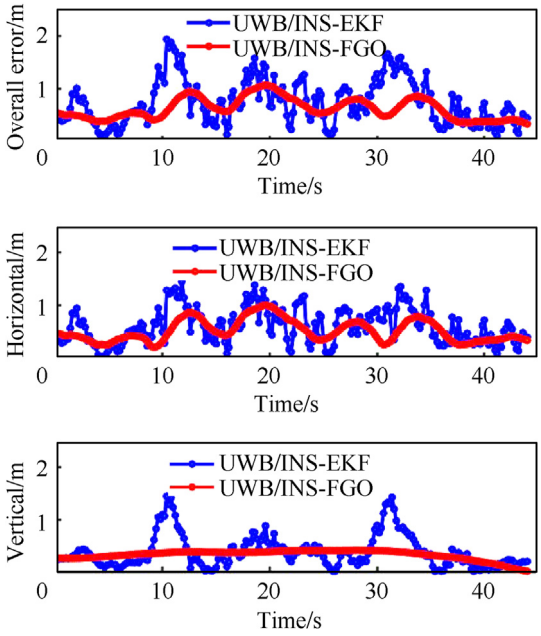

Fig. 14. Positioning results and errors of two methods under challenging scenario.

Table 5
Positioning performance of two methods under indoor challenging scenario.

Position errors/meters		EKF	FGO
Overall error	Mean	0.745	0.627
	Standard deviation	0.422	0.196
Horizontal component	Mean	0.610	0.519
	Standard deviation	0.335	0.206
Vertical component	Mean	0.386	0.335
	Standard deviation	0.314	0.092

4.4. Resilient FGO under indoor challenging scenario

The above experiments have discussed the necessary of signal classification and noise prediction. In this subsection, the resilient FGO method involving the two-phase CNNs structure is tested. After utilizing the signal classification network to classify the environment conditions of UWB, the noise prediction network is used to output the detailed value of UWB measurement noise and the prediction results is shown in Fig. 15. As the input noise covariance matrix in FGO is the square of the range measurement error, to satisfy this demand, the predicted value of measurement covariance is also the square of the actual noise. It should be noted that the prediction results also corresponded to the relationship between anchor location and NLOS signals to some extent. For example, the reflections of $A1$ focused on the beginning and the end of the flight, and the signals of $A3$ are easy to be blocked or reflected during the mid-time. As the $A4$ anchor are located at the top center of the room, the UAV can receive its signal directly without any block or reflection during the whole flight. It results a quite small measurement noise which corresponding to the result in the noise prediction network.

To evaluate the superiority of resilient FGO method, different fixed measurement noise covariances are employed in classical FGO for comparison with the resilient FGO. The fixed measurement noise covariances are from 0.4 to 1.0 m with an interval of 0.2 m.

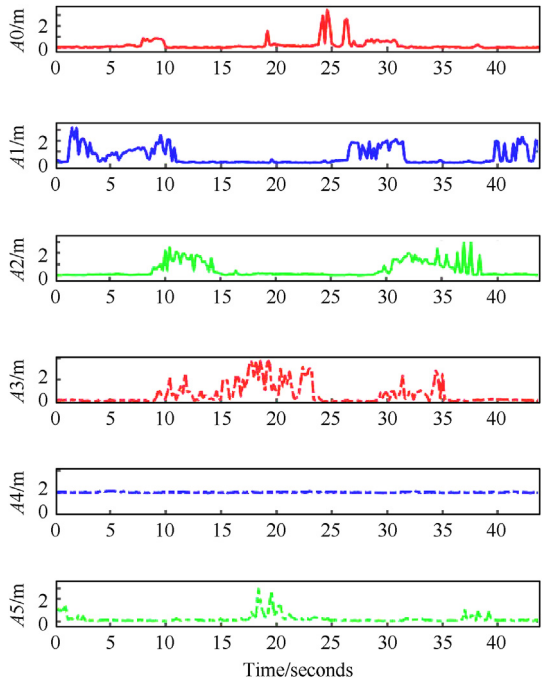

Fig. 15. Prediction value of measurement noise of INS/UWB integrations using Noise Prediction Network.

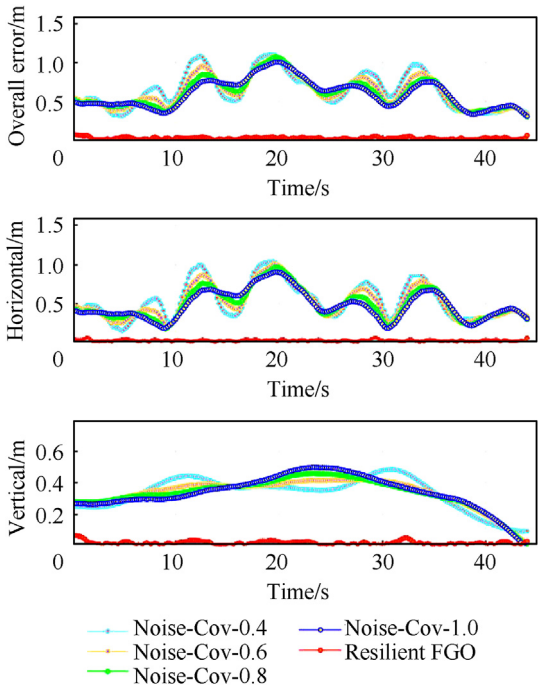

Fig. 17. Positioning performance and errors of FGO methods with different noises under challenging scenario.

The trajectory and positioning results under this challenging scenario are shown in Figs. 16 and 17. The detailed statistical data about the corresponding positioning errors of every FGO method are shown in Table 6.

As shown in the above figure, on one hand, for those FGO results with fixed measurement noises, the positioning performance is different in different period. It is difficult to conclude that which one is better. A bigger noise covariance could reduce the impact of fault measurement. However it would decrease the positioning accuracy in nominal scenario. On the other hand, the positioning accuracy of resilient FGO method is much better than all those method with fixed measurement noises.

As show in Table 6, it can be seen that for the classical FGO methods which with the fixed settings of measurement noise, the positioning performance are basically unchanged and the positioning errors fluctuate around 0.50 m and 0.33 m in horizontal and vertical directions, respectively. It should be addressed that it is difficult to complete the indoor work based on this positioning accuracy. After applying the deep learning based resilient stochastic model, it is encouraging that the positioning error in horizontal and vertical direction are sharply decreased to 0.027 m and 0.016 m, respectively. Meanwhile, the overall standard deviation is about 0.017 m, which indicates that the error distribution has become more precise and compact. The resilient FGO method for tightly coupled INS/UWB integration is verified in this indoor challenging scenario. The accuracy improvements can meet the performance requirements of high precision indoor navigation task.

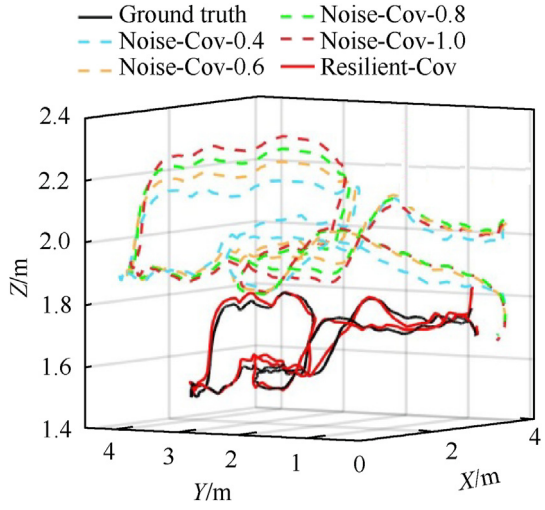

Fig. 16. Fight trajectory and positioning results with different measurement noise settings.

5. Conclusions

(1) The tightly coupled INS/UWB integrated system based on resilient factor graph optimization (FGO) structure is proposed in this paper to overcome the challenge of complex indoor environment to realize the high precision indoor UAV navigation. The deep learning method is introduced into the FGO method to identify the UWB NLOS signals and predict precise measurement noise.

(2) Due to the limited features, the UWB signals classification is difficult to achieve a desired success rate. Hence the implementation of resilient stochastic model is designed into two phases, one for identify the NLOS signals and the other one for predicting the measurement noises. The residual NLOS signals in the first phase are regarded as noise in the second phase to reduce their impact on positioning performance.

(3) The proposed resilient tightly-coupled INS/UWB FGO method is tested on UAV platform under actual indoor challenging environment. The experiment results verified its superiority compared to classical EKF method and noise-fixed FGO method. Under signal block and reflection scenarios, the self-tuning measurement noise covariance can

Table 6
Positioning performance of fgo methods with different noises under challenging scenario.

Position errors/meters		Noise-Cov-0.4	Noise-Cov-0.6	Noise-Cov-0.8	Noise-Cov-1.0	Resilient FGO
Overall error	Mean	0.645	0.627	0.614	0.601	0.038
	Standard deviation	0.225	0.198	0.187	0.181	0.017
Horizontal component	Mean	0.540	0.519	0.499	0.484	0.027
	Standard deviation	0.228	0.206	0.192	0.181	0.015
Vertical component	Mean	0.334	0.335	0.335	0.339	0.016
	Standard deviation	0.103	0.092	0.096	0.108	0.013

effectively enhance the ability of FGO to deal with NLOS signals and uncertain noises. The overall errors can be decreased from about 0.60 m to centimeter-level.

Declaration of competing interest

The authors declare that they have no known competing financial interests or personal relationships that could have appeared to influence the work reported in this paper.

Acknowledgements

The authors would like to acknowledge National Natural Science Foundation of China (Grant No. 62203111), the Open Research Fund of State Key Laboratory of Information Engineering in Surveying, Mapping and Remote Sensing, Wuhan University (Grant No. 21P01) and the Foundation of Key Laboratory of Micro-Inertial Instrument and Advanced Navigation Technology, Ministry of Education, China (Grant No. SEU-MIAN-202101) to provide fund for conducting experiments.

References

[1] Meng Q, Hsu L. Resilient interactive sensor-independent-update fusion navigation method. IEEE Trans Intell Transport Syst 2022;23(9):16433–47.
[2] Yang Y. Resilient PNT concept frame. Journal of Geodesy and Geoinformation Science 2019;2(3):1–7.
[3] Jurado J, Raquet J, Kabban CMS. Single-filter finite fault detection and exclusion methodology for real-time validation of plug-and-play sensors. IEEE Trans Aero Electron Syst 2021;57(1):66–75.
[4] Patle BK, Ganesh BL, Pandey A, Parhi D, Jagadeesh A. A review: on path planning strategies for navigation of mobile robot. Defence Technology 2019;15(4):582–606.
[5] Kassas ZM, Closas P, Gross J. Navigation systems panel report navigation systems for autonomous and semi-autonomous vehicles: current trends and future challenges. IEEE Aero Electron Syst Mag 2019;34(5):82–4.
[6] Li B, Yang ZP, Chen DQ, Liang SY, Ma H. Maneuvering target tracking of UAV based on MN-DDPG and transfer learning. Defence Technology 2021;17(2):457–66.
[7] Yang B, Guo L, Li F, Ye J, Song W. Vulnerability assessments of electric drive systems due to sensor data integrity attacks. IEEE Trans Ind Inf 2020;16(5):3301–10.
[8] Ai YB, Rui T, Yang XQ, He JL, Fu L, Li JB, Lu M. Visual SLAM in dynamic environments based on object detection. Defence Technology 2021;17(5):1712–21.
[9] Choi YJ, Ramatryana INA, Shin SY. Cellular communication-based autonomous UAV navigation with obstacle avoidance for unknown indoor environments. International Journal of Intelligent Engineering and Systems 2021;14(2):344–52.
[10] Fu L, Gu WB, Li W, Chen L, Ai YB, Wang HL. Bidirectional parallel multi-branch convolution feature pyramid network for target detection in aerial images of swarm UAVs. Defence Technology 2021;17(4):1531–41.
[11] Ahmed SA, Mohsin M, Ali SMZ. Survey and technological analysis of laser and its defense applications. Defence Technology 2021;17(2):583–92.
[12] Shakhatreh H, Khreishah A, Khalil I. Indoor mobile coverage problem using UAVs. IEEE Syst J 2018;12(4):3837–48.
[13] Zhang K, Chen P, Ma T, Gao S. On-demand precise tracking for energy-constrained UAVs in underground coal mines. IEEE Trans Instrum Meas 2022;71:1–14. https://doi.org/10.1109/TIM.2022.3146925. Art no. 5500814.
[14] Zahran S, Moussa AM, Sesay AB, El-Sheimy N. A new velocity meter based on Hall effect sensors for UAV indoor navigation. IEEE Sensor J 2019;19(8):3067–76.
[15] Matos-Carvalho JP, Santos R, Tomic S, Beko M. GTRS-based algorithm for UAV navigation in indoor environments employing range measurements and odometry. IEEE Access 2021;9:89120–32.
[16] Jia J, Guo K, Li W, Yu X, Guo L. Composite filtering for UWB-based localization of quadrotor UAV with skewed measurements and uncertain dynamics. IEEE Trans Instrum Meas 2022;71:1–13. https://doi.org/10.1109/TIM.2022.3151934. Art no. 1002313.
[17] Teulière C, Marchand E, Eck L. 3-D model-based tracking for UAV indoor localization. IEEE Trans Cybern 2015;45(5):869–79.
[18] Zhang Y, Tan X, Zhao C. INS/UWB integrated pedestrian positioning for robust indoor environments. IEEE Sensor J 2020;20(23):14401–9.
[19] Wang C, Xu A, Kuang J, Sui X, Hao Y, Niu X. A high-accuracy indoor localization system and applications based on tightly coupled INS/UWB/floor map integration. IEEE Sensor J 2021;21(16):18166–77.
[20] Jiang C, Shen J, Chen S, Chen Y, Liu D, Bo Y. UWB NLOS/LOS classification using deep learning method. IEEE Commun Lett 2020;24(10):2226–30.
[21] Yang X, Wang J, Song D, Feng B, Ye H. A novel NLOS error compensation method based IMU for UWB indoor positioning system. IEEE Sensor J 2021;21(9):11203–12.
[22] Guo SL, Sun YJ, Chang LM, Li Y. Robust cubature Kalman filter method for the nonlinear alignment of SINS. Defence Technology 2021;17(2):593–8.
[23] Raja G, Suresh S, Anbalagan S, Ganapathisubramaniyan A, Kumar N. PFIN: an efficient particle filter-based indoor navigation framework for UAVs. IEEE Trans Veh Technol 2021;70(5):4984–92.
[24] You W, Li F, Liao L, Huang M. Data fusion of UWB and IMU based on unscented kalman filter for indoor localization of quadrotor UAV. IEEE Access 2020;8:64971–81.
[25] Chatzi EN, Smyth AW. The unscented Kalman filter and particle filter methods for nonlinear structural system identification with non-collocated heterogeneous sensing. Struct Control Health Monit 2009;16(1):99–123.
[26] Wen W, Bai X, Kan YC, Hsu L. Tightly coupled GNSS/INS integration via factor graph and aided by fish-eye camera. IEEE Trans Veh Technol 2019;68(11):10651–62.
[27] Li X, Wang Y. Research on a factor graph-based robust UWB positioning algorithm in NLOS environments. Telecommun Syst 2021;76(2):207–17.
[28] Qin T, Li P, Shen S. VINS-mono: a robust and versatile monocular visual-inertial state estimator. IEEE Transactions on Robotics 2018;34(4):1004–20.
[29] Forster C, Carlone L, Dellaert F, Scaramuzza D. IMU preintegration on manifold for efficient visual-inertial maximum-a-posteriori estimation. In: Proceedings of robotics: science and systems, rome, Italy; 2015. Jul.
[30] Song Y, Hsu LT. Tightly coupled integrated navigation system via factor graph for UAV indoor localization. Aero Sci Technol 2020;108(2021):106370.
[31] Peynot T, Fitch R, McAllister R, Alempijevic A. Resilient navigation through probabilistic modality reconfiguration. In: Proceedings of intelligent autonomous systems 12, jeju island, korea; 2012. p. 75–88. June.
[32] Jurado JD. Autonomous and resilient management of all-source sensors for navigation assurance. Ph.D. dissertation. Ohio,USA: Dept. Air Force, Air Force Institute of Technology; 2019.
[33] Zwirello T, Schipper Harter M, Zwick T. UWB localization system for indoor applications: concept, realization and analysis. J. Elect. Comput. Eng. 2012;2012(5):849638.